Reduction of Particle Contamination on Air Bearing Sliders Part I: Wall Profile and

Crown Effects

Xinjiang Shen, Mike Suk and David B. Bogy

ABSTRACT

Due to the transverse flow of the air at the etch steps in current etched-cavity slider air bearing designs in hard disk drives, a contamination particle's flying path in the air bearing can be modified by changing the slider's wall profiles and crown. This will influence the particle contamination on the slider. In this study, it is shown that the wall profile has a major effect on the particle's path in a slider/disk interface and that one may optimize the wall profiles of a slider to reduce a particle's likehood of contacting the slider as it passes through the air bearing. It has the potential to minimize the effect of particle contamination on the slider's flying behavior. Also, by increasing the crown of the slider, one can increase its pitch angle and also reduce the particle contamination on the air bearing.

1. Introduction

To achieve the high data density of one terabit per square inch in hard disk drives, the flying height of the air bearing must be less than 5nm. At such low flying heights contamination particles are very likely to enter the spacing and accumulate on the air bearing slider. The motion of a particle moving from the leading edge to the trailing edge of an air bearing is quite difficult to describe due to the various parameters which may affect the forces acting on the particle. These forces depend

on the particle's size, density and the air velocity and pressure fields in the air-bearing. It is desirable to have the particles pass through the head disk interface without contaminating the air bearing. As shown by the authors in [1] the transverse flow in the air bearing at the etch step has an important effect on a particle's flying path. This transverse air flow can be changed by modifying the wall profiles and crown of a slider. By retarding a particle's motion toward the air bearing, one may reduce the particle's probability of contaminating the slider.

In this paper we study some three-dimensional effects on a particle's flying path and the contamination profiles on slider air bearings with different wall profiles and crowns. Since the number density of the particles is small, collisions between the particles are assumed to have negligible effect and thus are neglected in this investigation. Furthermore, adhesion of the particles on first impact with the slider or disk is assumed. The air bearing equation, including some three-dimensional flow effects [1], is used in this study to calculate the forces on the motion of a particle within an air-bearing based on previous work [2-7]. We then choose some contemporary slider designs and show that modification of the wall profiles causes less force on particles, thereby causing fewer particles to contaminate the air bearing. Our results also show that increasing a slider's crown not only increases its pitch angle, but also reduces a particle's likelihood of contaminating the slider's air bearing.

2.   Transverse Flow Effects in Air-bearing Flow Analysis

In order to determine the trajectory of a particle within an air-bearing we must first determine the spacing between the slider and disk surfaces as well as the pressure and velocity fields in the bearing. For a complex slider design with etch steps, the spacing between the slider and the disk surfaces varies abruptly in places, introducing

local three-dimensional airflow. Since the spacing is about three to five orders of magnitude less than the slider's lateral dimensions, we retain the following assumptions:

(1) The pressure gradient in the transverse direction is negligible; therefore, the pressure field calculated from the Reynolds equation is considered to be valid.

(2) The transverse air velocity in the step regions is not negligible although it is small compared to the in-plane velocity of the air.

For different slip boundary conditions required by rarefaction effects at high Knudsen numbers, the momentum equations of the air film have different solutions. Here we assume the first order slip condition [8], which is expressed by

$$u_g\big|_{z=0} = U + \lambda \frac{\partial u_g}{\partial z}\bigg|_{z=0} \tag{1}$$

$$u_g\big|_{z=h} = -\lambda \frac{\partial u_g}{\partial z}\bigg|_{z=h} \tag{2}$$

$$v_g\big|_{z=0} = V + \lambda \frac{\partial v_g}{\partial z}\bigg|_{z=0} \tag{3}$$

$$v_g\big|_{z=h} = -\lambda \frac{\partial v_g}{\partial z}\bigg|_{z=h} \tag{4}$$

where h is the local height of the air-bearing; U, V are the speeds of the disk in the x and y directions, and λ is the mean free path of the air. Using these boundary conditions, we obtain for the in-plane non-dimensional form of the velocity components of the air

$$U_g = \frac{P_0}{2\rho_g U^2}\frac{h_m}{l}\mathrm{Re}_h\frac{\partial P}{\partial X}\left(Z^2 - ZH - Kn_hH\right) + \left(1 - \frac{Kn_h + Z}{2Kn_h + H}\right) \tag{5}$$

$$V_g = \frac{P_0}{2\rho_g U^2}\frac{h_m}{l}\mathrm{Re}_h\frac{\partial P}{\partial Y}\left(Z^2 - ZH - Kn_hH\right) + \frac{V}{U}\left(1 - \frac{Kn_h + Z}{2Kn_h + H}\right) \tag{6}$$

3

where P is the dimensionless pressure, or pressure divided by the ambient pressure P_0;

$H = \dfrac{h}{h_m}$ is a non-dimensional spacing of the air-bearing; $Kn_h = \dfrac{\lambda}{h_m}$ is the Knudsen

number defined in terms of the minimum spacing height h_m. Since we continue to

assume that the pressure gradient in the z direction is negligible, the pressure field of

the air-bearing, P, can still be obtained from the Reynolds equation

$$\sigma \frac{\partial PH}{\partial T} = \frac{\partial}{\partial X}\left(QPH^3 \frac{\partial P}{\partial X} - \Lambda_x PH\right) + \frac{\partial}{\partial Y}\left(QPH^3 \frac{\partial P}{\partial Y} - \Lambda_y PH\right), \qquad (7)$$

where $\sigma = \dfrac{12\mu_g \hat{\Omega} l^2}{p_0 h_m^2}$ is the squeeze number; $Q = 1 + 6a\dfrac{Kn_h}{PH}$ is the flow factor for the

first order slip model; $a = \dfrac{2-\alpha}{\alpha}$ and α is the accommodation factor; and Λ_x and Λ_y

are the bearing numbers $\Lambda_x = \dfrac{6\mu_g U l}{p_0 h_m^2}$ and $\Lambda_y = \dfrac{6\mu_g V l}{p_0 h_m^2}$.

For the transverse velocity of the air, w, the boundary conditions are

$$w\big|_{z=0} = 0 \qquad (8)$$

$$w\big|_{z=H} = 0 \qquad (9)$$

Let $w = W(Z)(H - Z)U$, and substitute this into the continuity equation to obtain

$$\frac{\partial U_g}{\partial X} + \frac{\partial V_g}{\partial Y} - \frac{l}{h_m}\frac{\partial[W(H-Z)]}{\partial Z} = 0 \qquad (10)$$

By substituting U_g, V_g from Eqs. (5) and (6) into Eq. (10), one may integrate the result

to obtain an   analytical expression for the transverse velocity of the air in the air-

bearing.

3.   **Particle Kinetics Equations**

The governing equations for a particle moving in air can be written as

$$\frac{d\bar{x}}{dt} = \bar{v}$$

(11)

$$m\frac{d\bar{v}}{dt} = \bar{f}$$

(12)

where $\bar{x}$ and $\bar{v}$ are the position and velocity vectors of the particle, respectively; m represents the mass of the particle; $\bar{f}$ includes the forces of drag, Saffmann lift, Magnus lift and gravity acting on the particle. The electrostatic and molecular forces between particles and slider surfaces are neglected. The details of the forces have been studied by Zhang and Bogy [5], and so they are only briefly outlined here:

(1)   Drag force

For a rigid spherical particle moving in airflow, the drag force can be expressed as

$$\bar{f}_d = \frac{\pi}{8} C_d C_w \rho_g d^2 \left\| \bar{u}_g - \bar{u}_p \right\| \left(\bar{u}_g - \bar{u}_p \right)$$

(13)

where C_d is the drag coefficient; C_w is the coefficient of the wall effects which tends to unity when the particle is far enough away from the wall; d is the diameter of the sphere; ρ_g is the density of the air; $\bar{u}_g$ and $\bar{u}_p$ are the velocity of the air and sphere, respectively.

(2)   Saffmann lift force

The lift force acting on a spherical particle in a linear shear flow can be expressed as

$$f_{SL} = \frac{9}{\pi} J\mu R^2 \Delta U \left(\frac{\rho_g G}{\mu} \right)^{1/2}$$

(14)

where μ is the viscosity of the air; ΔU is the velocity of the sphere relative to the airflow, which is given by $\Delta U = \dfrac{\left(\bar{u}_p - \bar{u}_g \right) \cdot \bar{u}_g}{\left\| \bar{u}_g \right\|}$; G is the magnitude of the airflow shear

rate calculated by $G = \dfrac{\bar{u}_g \cdot \dfrac{\partial \bar{u}_g}{\partial z}}{\left\| \bar{u}_g \right\|}$; J is expressed by Cox and Hsu [9]

as $J = \dfrac{\pi^2}{16}\left(\dfrac{1}{\varepsilon} + \dfrac{11}{6}l_w^*\right)$. For a sphere far away from the wall J converges to Saffmann's

value of 2.255. When the sphere is close to the wall J depends on the ratio,

$\varepsilon = \dfrac{\left(\mathrm{Re}_G\right)^{1/2}}{\mathrm{Re}_S}$, and a non-dimensional distance $l_w^* = \left(\rho_g G / \mu\right)^{1/2} l_w$ in which l_w is the

distance between the sphere and wall. Here $\mathrm{Re}_s = \Delta U R \rho_g / \mu$ and $\mathrm{Re}_G = G R^2 \rho_g / \mu$.

(3) Magnus lift force

   The spinning of the particle and the air shear results in Magnus lift, which is

expressed as

$$f_m = \frac{\pi}{8}\rho_g d^3 \left\{ \left[\bar{\omega} \times \left(\bar{u}_p - \bar{u}_g\right)\right] \cdot \bar{e}_z + \frac{1}{2}\frac{\partial \bar{u}_g}{\partial z}\cdot\left(\bar{u}_p - \bar{u}_g\right)\right\} \tag{15}$$

where $\bar{\omega}$ is the angular velocity vector of the particle; $\bar{e}_z$ is the unit vector in the z

direction.

(4) Gravity force

   The gravity force is represented as

$$\bar{f} = \frac{4}{3}\pi R^3 \left(\rho_g - \rho_p\right)\bar{g} \tag{16}$$

where $\bar{g}$ is the acceleration due to gravity. The buoyancy force is also included in the

calculation although it is negligible compared to the gravity force.

For particle flow analysis the number and size distribution of the particles can, in principle, be determined from experiments. The particles are first assumed to be uniformly distributed above the disk surface with velocities close to the air-bearing's velocity where the particles are located, as determined by Eqs. (5) and (6). The particle's initial transverse velocity is assumed to be zero.

4.   Numerical Results and Discussions

To study the effects of the wall profile and crown the reference slider for our numerical simulations is shown in Figure 1. Its 3-D view is shown in Figure 2. From the reference air bearing surface to the first etch step, there is a slope, which is determined by various manufacturing processes. It is defined as a shallow step wall profile. There is also a wall profile from the shallow etch to the recess region of the slider. The reference slider's center trailing edge flying height is 26nm with a pitch angle of 56 μrad at a particular location on the disk. We examined three wall profiles in the numerical experiments. The first wall profile has two straight segments as shown in Fig. 3. The depth from the air bearing to the shallow step is 0.28 micron, The wall profile from the shallow step to the recess region is shown in Figure 4. For the second slider design, the curved wall profile shown in Figure 5 is used for the shallow step, while the straight wall profile in Figure 4 is again used from the shallow step to the recess.   The third slider has the curved wall profile in Figure 5 for the shallow step, while the curved wall profile shown in Figure 6 is used from the shallow step to the recess region of the slider. The flying characteristics of these three sliders are listed in Table 1. The nominal flying height of each slider is 26nm. Their pitch angles are 56, 62, 64 μrad , respectively.

The transverse air flow in the head disk interface is modified dramatically by the changes in the wall profile. Figure 7 shows that the transverse air flow velocity at the transition region of the slider with a straight wall profile is 0.17U in the middle of the spacing at y=0.2mm. The transverse air flow is as low as 0.02U at the same location for the slider with a curved wall profile. The two wall profiles corresponding to this major transverse air flow difference are shown in Figure 8. It is seen that the curved wall profile reduces the abrupt transverse flow dramatically. Due to the transverse air flow decrease, a 30nm particle can not easily fly toward the air bearing surface at the transition region of the slider and contaminate it. The 30nm particle's flying paths in these two air bearings are shown in Figure 9. The particle density is 4.25×10^3 kg/m^3. The particles are initially located at x=0.425mm, y=0.2mm and z=5hm. The particle in the air bearing with the straight wall profile flies toward the slider surface and contaminates it right after the transition region (Figure 9(a)). However, the same particle starting from the same position with the same condition for the curved profile passes through the head disk interface without touching the slider's surface, as illustrated in Figure 9(b).

For the particle contamination simulations, 864 30nm alumina particles were used. They were initially uniformly distributed close to the disk. Figure 10 shows the particle contamination profile for the original slider design. It is shown that many particles are deposited on the leading pad, and also on the trailing pad of the air bearing. In all, 237 particles adhered to the air bearing using the worst-case scenario. For the improved wall profile design, 76 particles were deposited on the air bearing, as shown in Figure 11. No particle is shown on the trailing pad of this slider, and many fewer particles are collected on the leading pad of the slider.

To further modify the transverse air flow pattern in an air bearing one may increase the crown to reduce the drag force acting on a particle flying in the air bearing. Figure 12 shows the particle contamination profile on two slider designs with different crowns. The first slider has a crown of 5nm, while the second slider has a crown of 20nm. They fly at 5 and 7nm, respectively. Increasing the crown also increases the pitch angle of the slider, which is desirable for its dynamic performance; but what is the effect of increasing the pitch angle of a slider on particle contamination? From the particle contamination profiles shown in Figure 12 one may see that many fewer particles are collected on the air bearing of the slider with 20nm crown. And also, there is no particle at the transition region of the inside leading pad on the 20nm crown slider while many particles are observed there on the slider with 5nm crown. Even though the slider with 20nm crown has a higher pitch angle than the slider with 5nm crown, the total number of particles deposited on the air bearing of the 20nm crown slider is 7% less than the number of particles on the other slider, as shown in Table 2.

5.   Conclusions

Due to the effect of the air's transverse flow on a particle's flying behavior in the air bearing, one may modify a particle's flying path by changing the wall profiles and crown of a slider. The current study found that the wall profile can have a large effect on particle contamination profile on a slider. The curved wall profile is advantageous for reducing particle contamination on the slider's air bearing. One such wall profile is shown to reduce the air's transverse flow velocities at the transition

regions of a slider. For this slider with curved wall profiles, a 70% reduction of the small particle contamination is predicted by the numerical experiments. Also, increasing the crown of a slider's air bearing, one not only increases the slider's pitch angle, but also reduces by 7% the particle contamination on the particular slider studied.

Acknowledgements

References

[1]   Shen, X.-J., Mike Suk and Bogy, D. B., 2003, "Study of Transverse Flow Effects on Particle Flows and Contamination of Air Bearing Sliders", Submitted to the ASME Journal of Tribology for Publication.

[2]   Liu, V. C., Pang, S. C. and Jew, H., 1965, "Sphere Grad in Flows of Almost -Free Molecules", Physics of Fluids, **8**(5), pp. 788-796.

[3]   Saffman, P. G., 1965, "The lift on a Small Sphere in A Slow Shear Flow", Journal of Fluid Mechanics, **22**, pp. 385-400.

[4]   Chen, X., 1996, "The Drag Force acting on a Spherical Non-evaporating or evaporating particle immersed into a rarefied plasma flow", Journal of Physics D: Applied Physics, **29**, pp. 995-1005.

[5]   Zhang, S. and Bogy, D. B., 1997, "Effects of Lift on the Motion of Particles in the Recessed Regions of a Slider", Physics of Fluids, **9**, pp. 1265-1272.

[6]   Zhang, S. and Bogy, D. B., 1997, "Slider Designs for Controlling Contamination," Journal of Tribology, **119**, pp. 537-540.

[7]   Xinjiang Shen and David B. Bogy, 2002**, "**Particle Flow and Contamination in Slider Air Bearings for Hard Disk Drives", ASME Journal of Tribology, **125**, pp. 358-363.

[8]   Burgdorder, A., 1959, "The Influence of the Molecular Mean Free Path on the Performance of Hydrodynamics Gas Lubricated Bearing", ASME Journal of Basic Engineering, **81**(1), pp.94-100.

[9]   Cox, R. G. and Hsu, S. K., 1977, "The Lateral Migration of Solid Particles in A Laminar Flow near a Plane", International Journal of Multiphase Flow, **3**, pp.201-222.
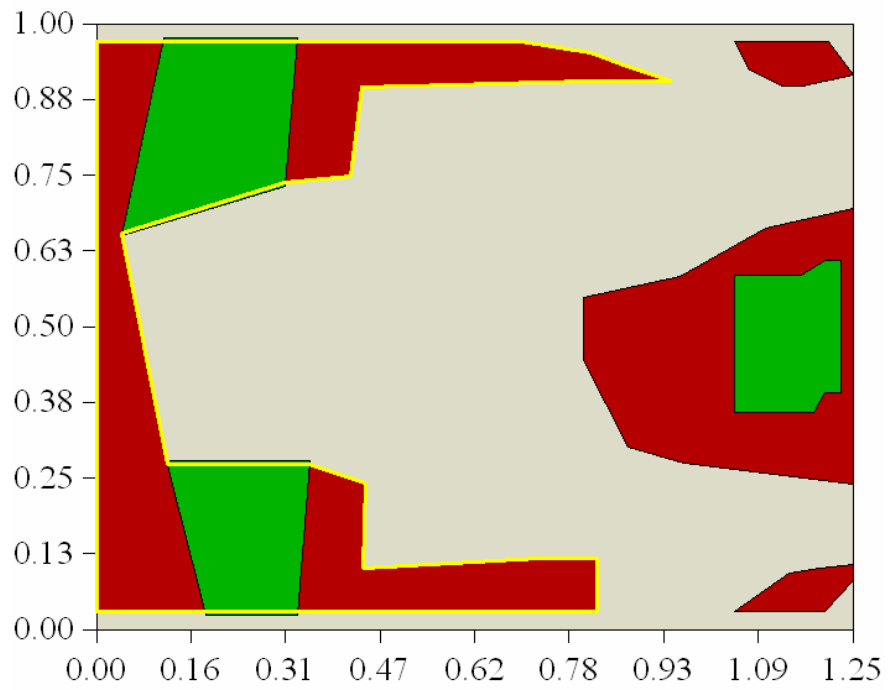
Figure 1. A reference slider used to study wall profile and crown effects

Shallow step wall profile
Wall profile from step to recess region
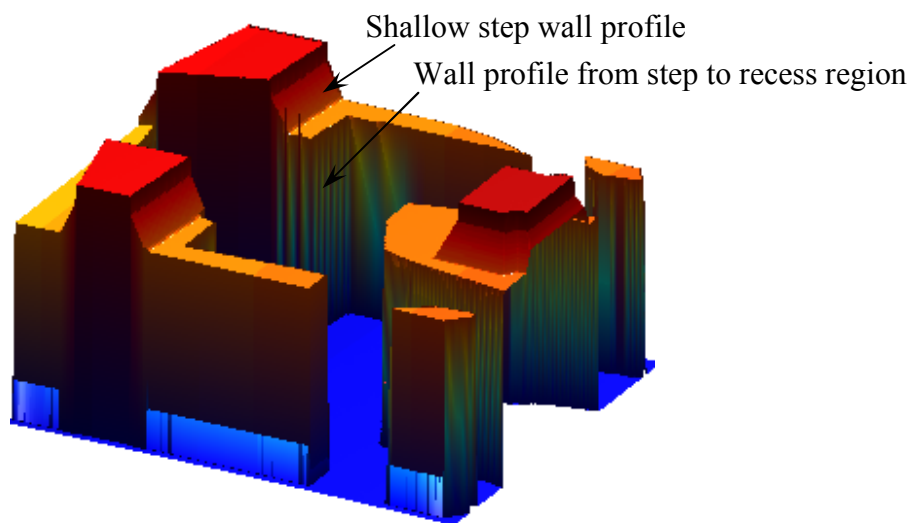
Figure 2. 3-D view of the reference slider with original wall profiles

12
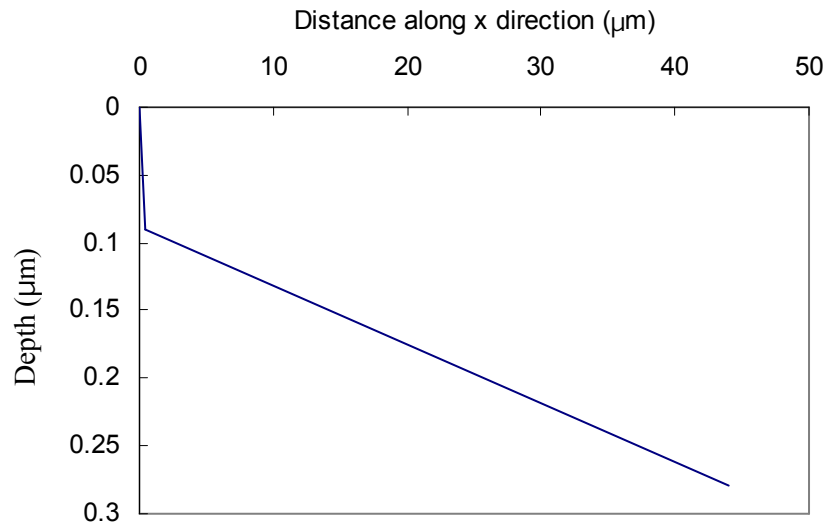
Figure 3. Straight segment shallow step wall profile
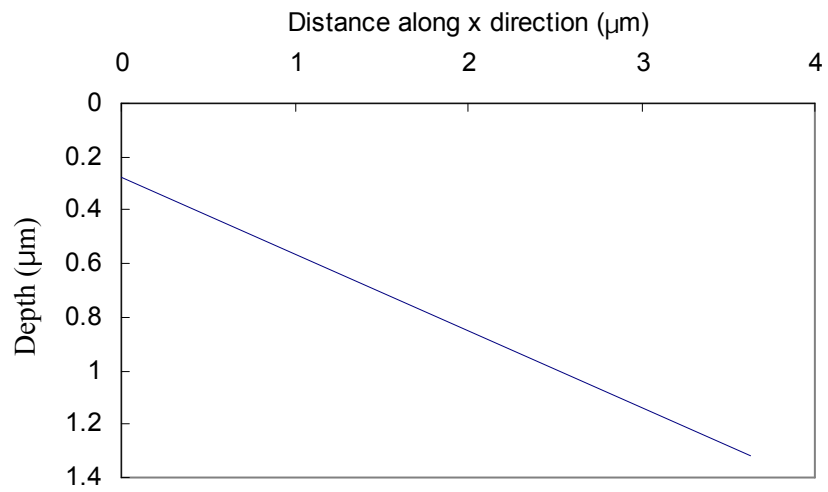
Figure 4. Straight wall profile from step to the recess region
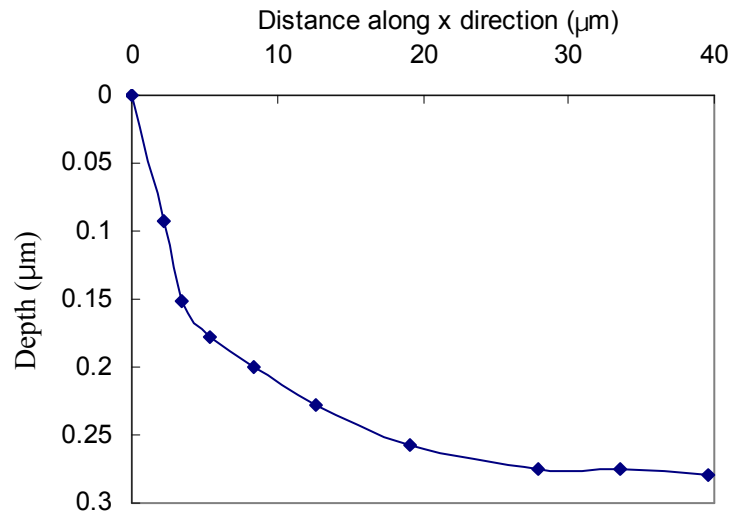
Figure 5. Curved wall profile for the shallow step
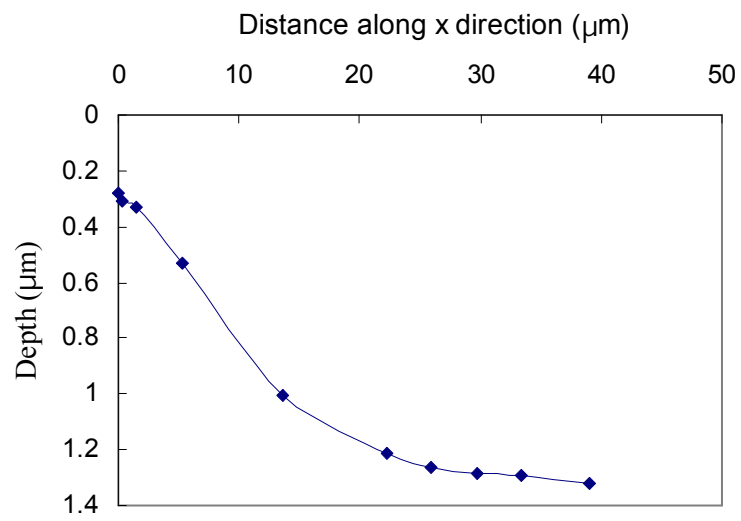
Figure 6. Curved wall profile from the shallow step to the recess region
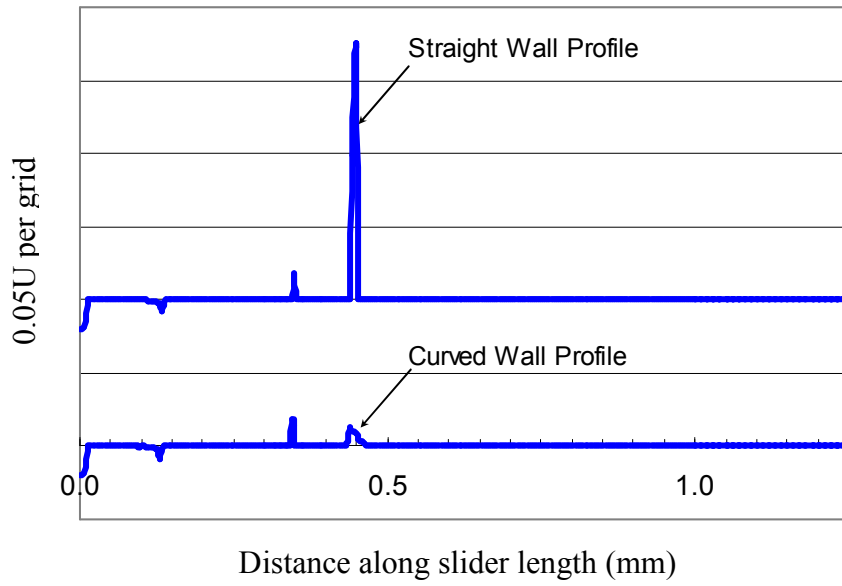
Figure 7. Comparison of transverse air velocities between straight and curved wall

profiles at 50% of the slider spacing at y=0.2mm
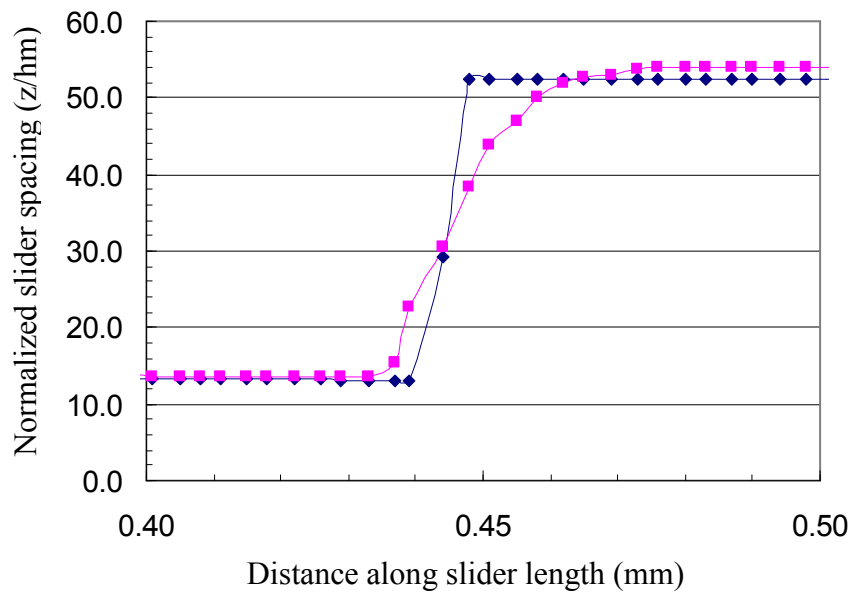
Figure 8. Slider spacing using straight and curved wall profiles at y=0.2mm
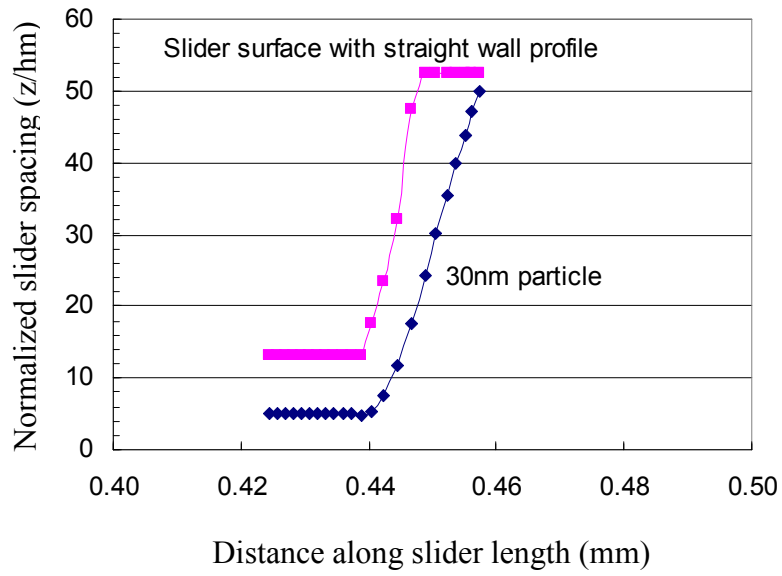
(a) Particle flying path in air bearing with straight wall profile
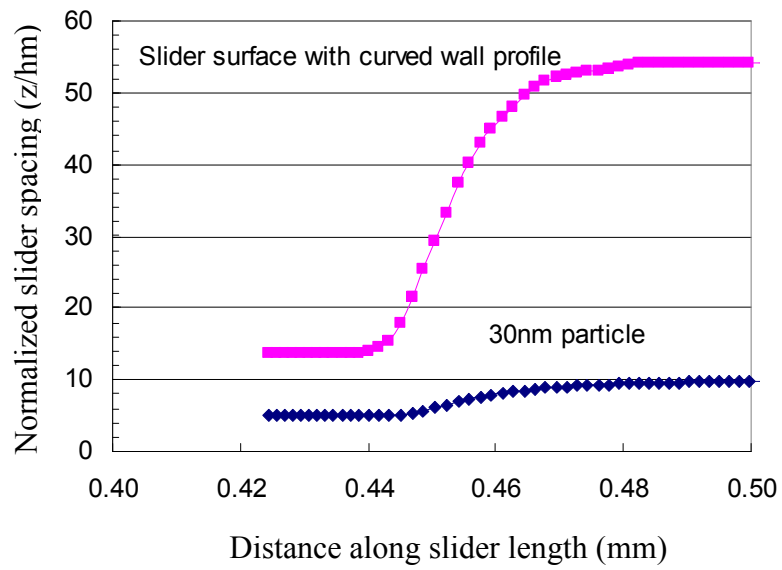
(b) Particle flying path in air bearing with curved wall profile

Figure 9. Particle flying paths under sliders with straight and curved wall profiles
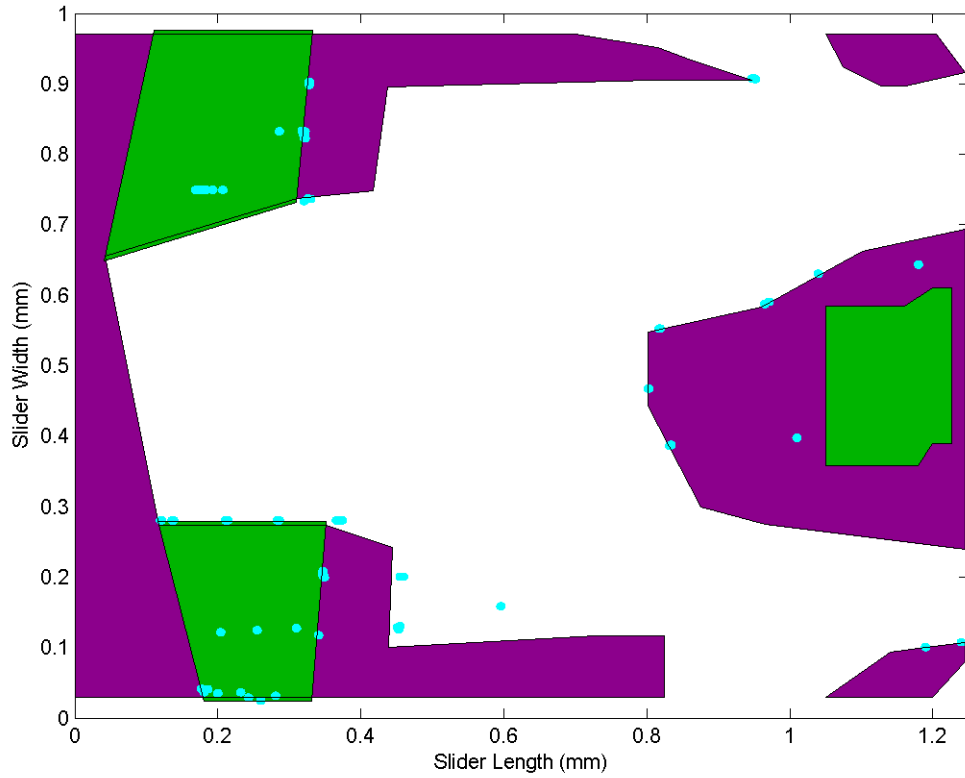
Figure 10. Particle contamination profile for the original slider design
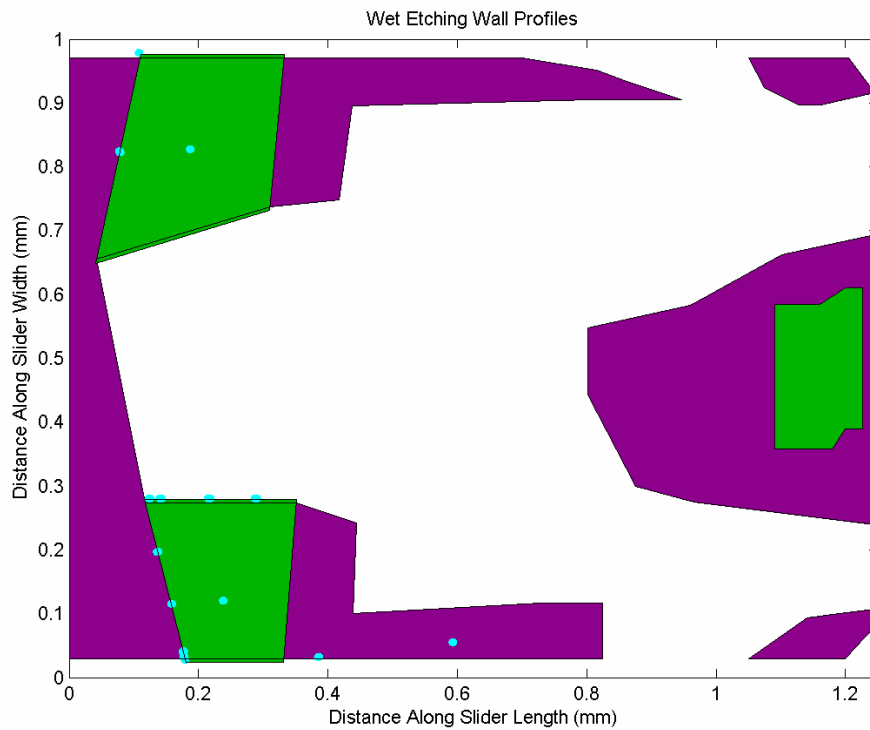
Figure 11. Particle contamination profile for the optimized wall profile slider design
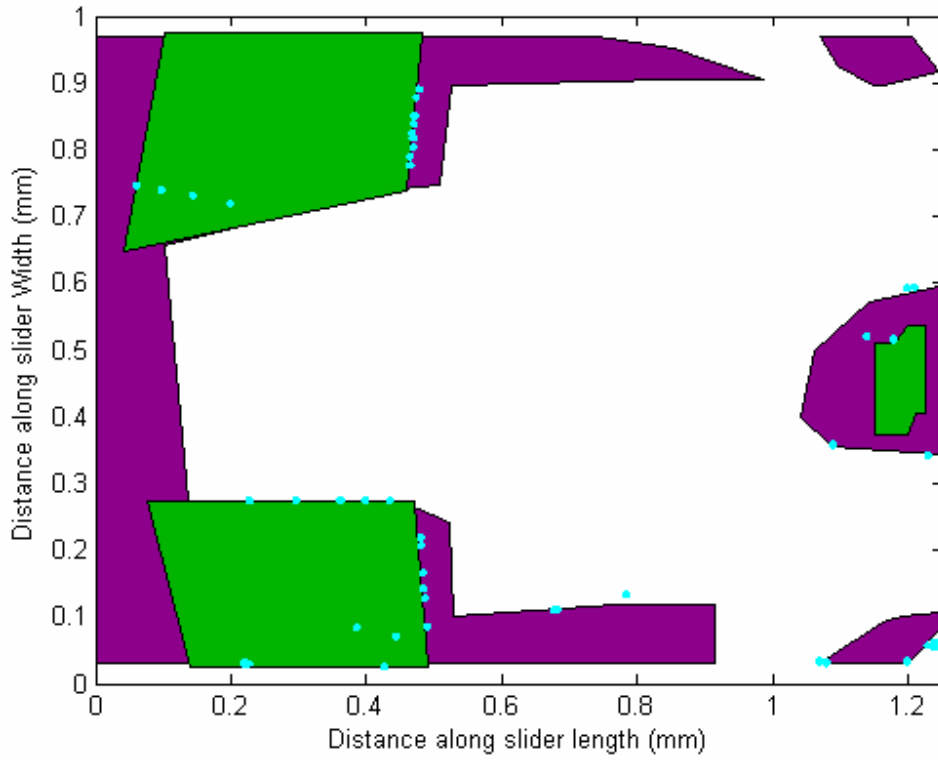
(a) Particle contamination profile on 5nm crown air bearing
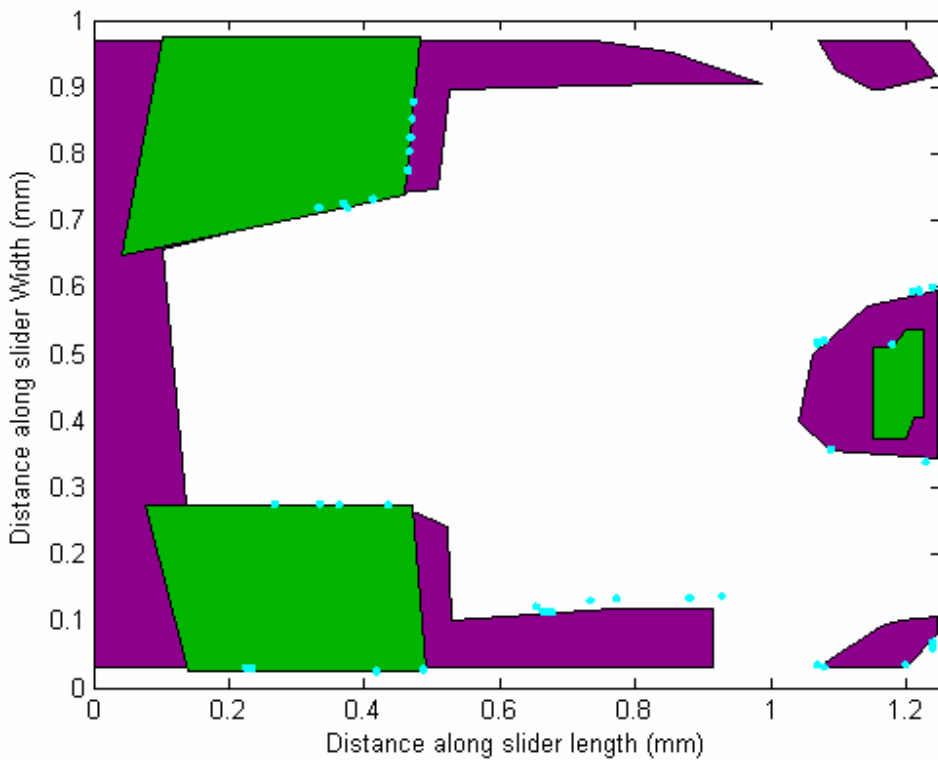
(b) Particle contamination profile on 20nm crown air bearing

Figure 12. Crown effects on particle contamination profile on slider air bearings

Table 1. Summary of wall profiles effect on particle contamination profiles on sliders

	Original Slider	Modified I	Modified II
FH (nm)	26	26	25.5
Pitch	56	62	64
Roll	-0.57	-4	-4
No. of particles on the slider (out of 864)	237	161	76

Table 2. Summary of crown effects on particle contamination profiles on sliders

Crown	5nm	20nm
FH (nm)	5	7
Pitch	150	166
Roll	0.82	1.6
No. of particles on the slider (out of 864)	169	157